Biophysical Journal, Volume *122*

Supplemental information

G-actin diffusion is insufficient to achieve F-actin assembly in fast-treadmilling protrusions

Ravikanth Appalabhotla, Mitchell T. Butler, James E. Bear, and Jason M. Haugh

Supporting Information

'G-actin diffusion is insufficient to achieve F-actin assembly in fast-treadmilling protrusions,' by Appalabhotla et al.

Text S1: Modeling Supplement

Supplemental Figures

Captions for Supplemental Movies S1-S5

Text S1: Modeling Supplement

1. General results for derivation of the general steady-state (pre-bleach) model

Our model is cast in terms of total G- and F-actin, which can exist in a variety of nucleotide- and regulatory protein-bound states. Here, we formulate the model with an accounting of all cytosolic states of G-actin, all states of F-actin, and all leading-edge membrane-bound states of G-actin. Modeling assumptions will be stated as they are invoked, so that the reader will know the generality of each set of equations.

Assumption 1.1: The cytoplasm of the non-adhesive region is homogenized into a single, continuous phase.

With this established, we define the cytosolic concentrations of G- and F-actin in various states i and j, respectively; their fluxes; the densities of leading-edge membrane-bound G-actin in various states n; and all of the sums thereof:

$$G = \sum_i G_i\,; \quad F = \sum_j F_j\,;$$

$$\mathbf{N}_G = \sum_i \mathbf{N}_{G,i}\,; \quad \mathbf{N}_F = \sum_j \mathbf{N}_{F,j}\,;$$

$$G_m = \sum_n G_{m,n}.$$

Because all F-actin moves together via retrograde flow, we can define the fluxes for each F-actin species and for total F-actin:

$$\mathbf{N}_{F,j} = \mathbf{V}_F F_j; \quad \mathbf{N}_F = \mathbf{V}_F F,$$

where $\mathbf{V}_F$ is the F-actin retrograde flow velocity vector (experienced by all F-actin species j). Next, rate terms are defined in order to construct the general conservation equations, with:

Assumption 1.2: Within the non-adhesive domain, rates of GFP-β-actin synthesis and degradation are negligible relative to those affecting actin dynamics.

Neglecting such terms, the bookkeeping equations are

$$\frac{\partial G_i}{\partial t} = -\nabla \cdot \mathbf{N}_{G,i} - \sum_j \left(r_{pol,ij} - r_{depol,ij}\right) + \sum_{k \neq i} \left(r_{interG,ki} - r_{interG,ik}\right);$$

$$\frac{\partial F_j}{\partial t} = -\nabla \cdot \mathbf{N}_{F,i} + \sum_i \left(r_{pol,ij} - r_{depol,ij}\right) + \sum_{k \neq j} \left(r_{interF,kj} - r_{interF,jk}\right);$$

$$\frac{dG_{m,n}}{dt} = \sum_i \left(r_{on,in} - r_{off,in}\right) - \sum_j r_{pol,m,nj} + \sum_{k\neq n} \left(r_{interM,kn} - r_{interM,nk}\right).$$

The rates are defined as:
$r_{pol,ij}$ is the rate of polymerization of G-actin species i to form F-actin species j;
$r_{depol,ij}$ is the rate of depolymerization of F-actin species j to form G-actin species i;
$r_{interG,ki}$ is the rate of interconversion from G-actin species $k \neq i$ to generate G-actin species i;
$r_{interF,kj}$ is the rate of interconversion from F-actin species $k \neq j$ to generate F-actin species j;
$r_{on,in}$ is the rate of G-actin species i association to form membrane-bound species n;
$r_{off,in}$ is the rate of G-actin species i dissociation from membrane-bound species n;
$r_{pol,m,nj}$ is the rate of G-actin transfer from membrane-bound species n to form F-actin species j; and
$r_{interM,kn}$ is the rate of interconversion from membrane-bound species $k \neq n$ to generate membrane-bound species n.
Flux balances at $x = 0$ are

$$N_{x,G,i}\big|_{x=0} = -\sum_n \left(r_{on,in} - r_{off,in}\right) - \sum_j N_{pol,c,ij};$$
$$N_{x,F,j}\big|_{x=0} = \sum_i N_{pol,c,ij} + \sum_n r_{pol,m,nj}.$$

Here, $N_{x,G,i}$ is the x-component of the flux for G-actin species i, $N_{x,F,j}$ is the x-component of the flux for F-actin species j, and $N_{pol,c,ij}$ is the flux of G-actin species i incorporation to form F-actin species j, directly from the cytosol. By summing these, we obtain

$$\frac{\partial G}{\partial t} = -\nabla \cdot \mathbf{N}_G - r_{pol} + r_{depol};$$
$$\frac{\partial F}{\partial t} = -\nabla \cdot \mathbf{N}_F + r_{pol} - r_{depol};$$
$$\frac{dG_m}{dt} = r_{on} - r_{off} - r_{pol,m};$$
$$N_{x,G}\big|_{x=0} = -r_{on} + r_{off} - N_{pol,c}; \quad N_{x,F}\big|_{x=0} = N_{pol,c} + r_{pol,m},$$

where

$$r_{pol} = \sum_i \sum_j r_{pol,ij}; \quad r_{depol} = \sum_i \sum_j r_{depol,ij};$$

$$r_{on} = \sum_n \sum_i r_{on,in}\,; \quad r_{off} = \sum_n \sum_i r_{off,in}\,; \quad r_{pol,m} = \sum_n \sum_j r_{pol,m,nj}\,;$$
$$N_{pol,c} = \sum_i \sum_j N_{pol,c,ij}.$$

Assumption 1.3: The system is at steady state:

$$\frac{\partial G_i}{\partial t} = \frac{\partial F_j}{\partial t} = \frac{dG_{m,n}}{dt} = 0.$$

With the densities of the membrane-bound states at steady state, we obtain

$$N_{x,F}\big|_{x=0} = -N_{x,G}\big|_{x=0} = N_{pol} = N_{pol,c} + r_{pol,m};$$

and, because the total actin in the cytosol (G- plus F-) is conserved,

$$\nabla \cdot (\mathbf{N}_G + \mathbf{N}_F) = 0.$$

Assumption 1.4: Gradients of total G- and F-actin are negligible in the y- and z-directions.

Hence, we can write

$$N_{x,G}(x) + N_{x,F}(x) = 0.$$

In the main text, we simplify the notation, with $N_{x,G} \to N_G$ and $N_{x,F} \to N_F$.

2. Additional analysis of FRAP model boundary conditions: $x = 0$

In the previous section we showed that, at steady state, the kinetics and spatial variations of G-actin nucleotide exchange, complex formation at the leading edge, and incorporation into F-actin need not be considered. In contrast, to predict FRAP kinetics, these aspects do need to be considered, especially as they relate to the boundary conditions for F- and G-actin at the leading edge ($x = 0$). Continuing from the preceding Section 1, additional assumptions used to formulate those boundary conditions will be stated as they are used.

The generalized fluxes of unbleached G- and F-actin at $x = 0$ are as follows; see the previous section for definitions.

$$N_{Gun}|_{x=0} = -\sum_i \left[\sum_n \left(r_{on,in} \frac{G_{un,i}}{G_i}\bigg|_{x=0} - r_{off,in} \frac{G_{mun,n}}{G_{m,n}} \right) - \sum_j N_{pol,c,ij} \frac{G_{un,i}}{G_i}\bigg|_{x=0} \right];$$
$$N_{Fun}|_{x=0} = \sum_j \left(\sum_i N_{pol,c,ij} \frac{G_{un,i}}{G_i}\bigg|_{x=0} + \sum_n r_{pol,m,nj} \frac{G_{mun,n}}{G_{m,n}} \right).$$

We proceed to write generalized unsteady balances for the unbleached forms of the membrane-bound species, valid after bleaching, after stating:

Assumption 2.1: Interconversion between membrane-bound states (e.g., nucleotide exchange) occurs at rates that are negligible compared to the rates of dissociation and elongation.

$$\frac{dG_{mun,n}}{dt} = \sum_i \left(r_{on,in} \frac{G_{un,i}}{G_i}\bigg|_{x=0} \right) - \left(\sum_i r_{off,in} + \sum_j r_{pol,m,nj} \right) \frac{G_{mun,n}}{G_{m,n}}.$$

With this formulation, we see that the mean lifetime of an unbleached G-actin molecule in membrane-bound state n is

$$\tau_n = \frac{G_{m,n}}{\sum_i r_{off,in} + \sum_j r_{pol,m,nj}}.$$

Assumption 2.2: $G_{mun,n}$ are quasi-steady, an approximation we consider valid for $t \gg \tau_n$.

Hence, we obtain

$$\frac{G_{mun,n}}{G_{m,n}} \approx \frac{\sum_i \left(r_{on,in} \frac{G_{un,i}}{G_i}\Big|_{x=0} \right)}{\sum_i r_{off,in} + \sum_j r_{pol,m,nj}} = \frac{\sum_i \left(r_{on,in} \frac{G_{un,i}}{G_i}\Big|_{x=0} \right)}{\sum_i r_{on,in}}.$$

Incorporating this result into the flux expressions, we obtain

$$-N_{Gun}|_{x=0} = N_{Fun}|_{x=0} = \sum_j \sum_i \left[\left(N_{pol,c,ij} + \sum_n r_{pol,m,nj} \frac{r_{on,in}}{\sum_i r_{on,in}} \right) \frac{G_{un,i}}{G_i}\bigg|_{x=0} \right].$$

Assumption 2.3: The soluble G-actin species at the leading edge are equally polymerizable.

Hence, we obtain the result used to formulate the boundary conditions in the text:

$$-N_{Gun}(0,t) = N_{Fun}(0,t) = \sum_j \left(N_{pol,c,ij} + \sum_n r_{pol,m,nj} \right) \frac{G_{un}}{G}\bigg|_{x=0} = N_{pol} \frac{G_{un}}{G}\bigg|_{x=0}.$$

With that done, we address now the validity of the three assumptions introduced in this section. The first two are readily addressed, considering published frequencies of profilin-G-actin dissociation and profilin-mediated transfer from polymerases (> 10 s^{-1}; references cited in the main text). By comparison, we acknowledge that the latter assumption is least general. It is accurate for scenarios with diffusion-limited polymerization ($g_{un}(0) \approx 0$); in that case, the boundary condition is equivalent to a Dirichlet boundary condition for g_{un} and flux-matching for f_{un}:

$$f_{un}(0,t) = \frac{D_G}{V_F}\frac{\partial g_{un}}{\partial x}\bigg|_{x=0} \quad \text{(diffusion-limited)}.$$

On the other hand, the assumption is not expected to be accurate for scenarios in which conversion to a polymerizable state of G-actin might be sluggish. We explore such a scenario in Section 5 of this supplement.

3. Additional analysis of FRAP model boundary conditions: $x = L$

In the main figures of the paper, FRAP predictions applied a Dirichlet (constant-value) boundary condition at $x = L$, assuming that the unbleached G-actin concentration there is maintained at the pre-bleach value:

$$g_{un}(L, y, t) = g(L).$$

The justification stated in the text is that the rear of the bleach zone backs up to the bulk of the cell volume and to a concentrated depot of disassembling F-actin. While we consider this assumption reasonable, we recognize that it represents an asymptotic limit of the true dynamics at that location, which is subject to diffusion of bleached G-actin into the cell body. In this section, we show that relaxing the constant-value assumption only modestly affects the prediction.

To address this, we constructed a 3D model in VCell that approximates the geometry of a cell adhered to a circular region of 30-μm diameter: a hemispherical (radius = 15 μm) cell body connected to a non-adhesive ring (outer radius = 25 μm, corresponding to L = 10 μm) (**Fig. S1A**). The lone species in this model is G-actin; to achieve a steady-state G-actin concentration field, G-actin is consumed by a 'sink' species confined to the membrane within the outermost 0.1 μm of the domain, and it is generated from a 'source' species confined to a ring on the bottom membrane with inner and outer radii of 14 and 15 μm at the interface between the cell body and non-adhesive region (**Fig. S1A**). The sink reaction is first-order with respect to G-actin concentration and sufficiently fast to drive the G-actin concentration to a very low value at the leading edge. The source reaction provides a constant flux, which determines the (arbitrary) scale of the concentration. VCell simulations were performed using the Fully-Implicit Finite Volume (variable time step) solver and a spatial discretization of 0.1 x 0.1 x 0.1 μm.

To closely match the two foundational scenarios presented in main **Fig. 4**, simulations were performed with 1) G-actin diffusivity $D_{G(c)}$ = 10.5 μm^2/s throughout the volume; and 2) G-actin diffusivity $D_{G(c)}$ = 3.0 μm^2/s throughout the volume plus radial advection velocity V_G = 0.90 μm/s in the non-adhesive region. For each simulation, rapid (0.1 s) bleaching was simulated as depicted in **Fig. S1B**, and the recovery of G-actin fluorescence at the center and rear of the bleach zone was quantified and adequately fit to a double-exponential function of time (**Fig. S1C**). Each of these was

then used to define a time-dependent boundary condition $g_{un}(L,t)$ in a 1D simulation, to be compared to the constant-value results at the level of leading-edge recovery (**Fig. S1D**). As expected, the time-dependent boundary condition yields slower recovery, but the $t_{0.5}$ values are only marginally increased (by 42% for DODL and by 25% for diffusion plus advection).

We note that F-actin was not included in these simulations, because accurate calculation of non-diffusive transport requires a prohibitively (in 3D) fine mesh to mitigate the issue of numerical diffusion. This is justified, insofar as G-actin recovery at the rear is concerned; on the timescale of that recovery, the depolymerization of unbleached F-actin near the leading edge is insignificant relative to diffusion of unbleached G-actin from the adjacent cell body.

We further note that we consider the conclusions from the 3D simulations to be conservative, in that the G-actin diffusivity was constant throughout the cell volume. In reality, diffusion within the cell body is expected to be faster than it is in the spillover region, where it is hindered by the excluded volume and tortuosity of the more tightly packed cytoplasm there (in no so small part because of the F-actin concentrated there). Faster diffusion in the cell body would cause faster recovery of $g_{un}(L,t)$ and therefore closer agreement with the leading-edge recovery predicted using the constant-value boundary condition.

4. Exploration of a two-state DODL model of G-actin transport: different diffusivities

Picking up from the end of Section 1 above, if one assumes Fickian diffusion for the cytosolic G-actin species i, we write

$$\mathbf{N}_{G,i} = -D_{Gi}\nabla G_i - \mathbf{V}_{Gi}G_i,$$

where D_{Gi} and $\mathbf{V}_G$ are the diffusivity and anterograde velocity vector of G-actin species i, respectively. Both of these potentially vary with position. Summing the fluxes, we obtain

$$\mathbf{N}_G = -D_G\nabla G - \mathbf{V}_G G;$$
$$\phi_i = \frac{G_i}{G};\quad D_G = \sum_i \phi_i D_{Gi};\quad \mathbf{V}_G = \sum_i (D_{Gi}\nabla\phi_i + \phi_i\mathbf{V}_{Gi}).$$

It is thus shown that there can be a diffusive contribution to the apparent anterograde flow vector (as defined). Considering that

$$\sum_i (\nabla\phi_i) = \nabla\left(\sum_i \phi_i\right) = 0,$$

we conclude that a nonzero contribution requires a substantial disparity in G-actin species i diffusivities and gradients of species i representation ϕ_i. The contribution will be positive/negative if and where the slower/faster diffusers are increasing in

representation as they move towards the leading edge. This suggests that a model considering slower- and faster-diffusing G-actin states might allow steady-state metrics to be achieved, with the faster-diffusing species taking the place of 'advection.' The question is whether or not this will result in slower FRAP, like the scenario of slow diffusion plus true vectorial transport.

To address this possibility, we develop a two-state model, with G-actin species concentrations, G_1 and G_2. They are governed by the steady-state conservation equations,

$$-\frac{dN_{G,1}}{dx} + k_{depol,1}F(x) - r_{12}(x) = 0;$$
$$-\frac{dN_{G,2}}{dx} + k_{depol,2}F(x) + r_{12}(x) = 0,$$

where $r_{12}(x)$ is the (as yet unspecified) net rate of interconversion from species 1 to species 2. To define the boundary conditions at the leading edge, we consider that each of the two species might (or might not) contribute to actin polymerization (through a combination of direct addition or via leading-edge polymerases), with

$$-N_{G,1}(0) = N_{pol,1};\ \ -N_{G,2}(0) = N_{pol,2};$$
$$N_F(0) = N_{pol} = N_{pol,1} + N_{pol,2} = V_F F_0.$$

Some general, steady-state results obtained by combining these equations are:

$$-N_{G,1}(x) = N_{pol,1} - \frac{k_{depol,1}}{k_{depol}} N_{pol}\left[1 - \exp\left(-\frac{k_{depol}}{V_F}x\right)\right] + \int_0^x r_{12}dx$$
$$-N_{G,2}(x) = N_{pol,2} - \frac{k_{depol,2}}{k_{depol}} N_{pol}\left[1 - \exp\left(-\frac{k_{depol}}{V_F}x\right)\right] - \int_0^x r_{12}dx$$

Summing these, we obtain the result from before,

$$-N_{G,1}(x) - N_{G,2}(x) = -N_G(x) = N_{pol}\exp\left(-\frac{k_{depol}}{V_F}x\right).$$

We now consider that only one of the two G-actin species is polymerizable. By inspection of the flux expressions, we see that the flux of the polymerizable form would be assisted by depolymerization directly into that form (or by depolymerization followed by a rapid conversion to that form) and by net conversion from the other, non-polymerizable species. Letting species 2 be the polymerizable form, only for the convenience that $r_{12}(x)$ is positive,

$$-N_{G,1}(x) = \int_0^x r_{12}dx\,;$$
$$-N_{G,2}(x) = N_{pol}\exp\left(-\frac{k_{depol}}{V_F}x\right) - \int_0^x r_{12}dx.$$

If we now assume that transport is by diffusion only, with constant diffusivities, we obtain

$$G_2(x) = G_2(0) + \frac{N_{pol}}{D_{G,2}}\frac{V_F}{k_{depol}}\left[1 - \exp\left(-\frac{k_{depol}}{V_F}x\right)\right] - \frac{D_{G,1}}{D_{G,2}}[G_1(x) - G_1(0)];$$

Given that there is an experimental constraint imposed on the value of $G(L) = G_1(L) + G_2(L)$, we reason that this system only makes sense if the polymerizable species 2 is the slower diffuser; the fast diffusing species 1 shortens the distance species 2 needs to diffuse.

For example, we considered a scenario wherein the species 1 consumption largely occurs close to the leading edge, such that species 1 has nearly constant flux elsewhere. To model this with a minimum number of parameters, we took

$$r_{12}(x) = r_m e^{-ax}(1 - e^{-bx}).$$

Note that the rate vanishes at $x = 0$, considering that we will assume that $G_1(0) \approx 0$ also (consistent with DODL assumptions; note that this also means that the polymerizability of species 1 is moot). The constants a and b are such that both aL and bL are large. Hence, we obtained

$$G_1(x) - G_1(0) = \frac{r_m}{D_{G,1}}\left[\frac{ax - 1 + e^{-ax}}{a^2} - \frac{(a+b)x - 1 + e^{-(a+b)x}}{(a+b)^2}\right],$$

and we used this result to obtain $G_2(x) - G_2(0)$ (with concentrations normalized by F_0). These results are shown in **Fig. S4A**, using parameter values consistent with the simulations presented in main **Fig. 4**: V_F = 0.2 μm/s, L = 10 μm, k_{depol} = 0.01 s^{-1}, $g(0) \approx 0$, and $D_{G,2}$ = 3 μm^2/s (matching our diffusion plus advection scenarios); to this we added $a = b$ = 3 μm^{-1} and $D_{G,1}$ = 12 μm^2/s, and finally r_m = 0.95 s^{-1} was fit to successfully match $g(L)$ = 0.15.

Another way to interpret this model is to set up the overall flux as before, with diffusion only:

$$-N_G(x) = D_{G,1}\frac{dG_1}{dx} + D_{G,2}\frac{dG_2}{dx} = N_{pol}\exp\left(-\frac{k_{depol}}{V_F}x\right),$$

or we can write

$$-N_G(x) = D_{G,2}\frac{dG}{dx} + \left(D_{G,1} - D_{G,2}\right)\frac{dG_1}{dx} = N_{pol}\exp\left(-\frac{k_{depol}}{V_F}x\right).$$

Interpreted this way, one might take the apparent diffusion coefficient as that of the slower, polymerizable species 2, and the second term on the left-hand side as the 'advective' flux:

$$V_G(x)G(x) = \left(D_{G,1} - D_{G,2}\right)\frac{dG_1}{dx}.$$

For the example given above, we calculated the apparent $V_G(x)$ and found that the values were ~ 1 μm/s, consistent with the analysis of the one-species model.

Having shown that a two-state, DODL model can sufficiently match typical experimental constraints at steady state, we turn our attention to the corresponding FRAP predictions, writing unsteady balances for the unbleached species (after bleaching),

$$\frac{\partial G_{un,1}}{\partial t} = D_{G,1}\nabla^2 G_{un,1} - r_{12}(x)\frac{G_{un,1}}{G_1};$$
$$\frac{\partial G_{un,2}}{\partial t} = D_{G,2}\nabla^2 G_{un,2} + k_{depol}F_{un} + r_{12}(x)\frac{G_{un,1}}{G_1}.$$

Applying associated boundary conditions, with the membrane-bound states considered quasi-steady as before, we have

$$N_{Fun}|_{x=0} = V_F F_{un}|_{x=0} = -N_{Gun,2}\Big|_{x=0} = D_{G,2}\frac{\partial G_{un,2}}{\partial x}\Big|_{x=0} = N_{pol}\frac{G_{un,2}}{G_2}\Big|_{x=0};$$
$$-N_{Gun,1}(0) = D_{G,1}\frac{\partial G_{un,1}}{\partial x}\Big|_{x=0} = 0,$$

together with the constant-value boundary conditions at $x = L$. This was applied to our example model of steady-state $r_{12}(x)$ in a 1D bleaching simulation (**Fig. S4B**). The results show that the two-species DODL model and the original DODL model with only one G-actin species yield similar FRAP predictions, unlike those generated when true advection was allowed. This is readily understood when one considers the effects of photobleaching on diffusive transport (explained also in the main-text Discussion): transient, large gradients of unbleached G-actin species yield fluxes that are much greater in magnitude than those associated with the steady state. As demonstrated above, we can construct an 'advective' flux and associated anterograde velocity $V_G(x)$ to achieve a reasonable steady state, but that $V_G(x)$ does not apply to unbleached G-actin in a diffusion-only model. The analogous construct for unbleached G-actin [which we might call $V_{Gun}(x,t)$] is transient and much larger during FRAP.

5. Exploration of a two-state model of G-actin transport: leading-edge polymerizability

We also applied a two-state G-actin transport model to relax the assumption that all of the G-actin at the leading edge is equally polymerizable. Specifically, we addressed whether or not a fairly slow conversion to a polymerizable form might cause slower FRAP with diffusion only. From the previous section, but with constant diffusivity D_G, we have at steady state,

$$D_G \frac{dG_1}{dx} = \int_0^x r_{12} dx\,;$$
$$D_G \frac{dG_2}{dx} = N_{pol} \exp\left(-\frac{k_{depol}}{V_F} x\right) - \int_0^x r_{12} dx.$$

Taking a simple, first-order rate of conversion in this case,

$$r_{12} = k_{12} G_1;$$
$$G_1(x) = G_1(L) \frac{\cosh(x/\lambda_1)}{\cosh(L/\lambda_1)}; \quad \lambda_1 = \sqrt{\frac{D_G}{k_{12}}}.$$

And,

$$G_2(x) = G_2(0) + \frac{N_{pol}}{D_G} \frac{V_F}{k_{depol}} \left[1 - \exp\left(-\frac{k_{depol}}{V_F} x\right)\right] - [G_1(x) - G_1(0)].$$

Obtaining suitable gradients with this model while keeping k_{12} low presents a trade-off. To optimize this, and also so that the flux of polymerizable, unbleached G-actin at the start of FRAP is zero (to give the best chance of slowing FRAP), we constrained

$$G_2(L) = G_2(0) = 0.$$

With this constraint, we set $G_1(L) = 0.15$ and the typical parameter values V_F = 0.2 μm/s, L = 10 μm, and k_{depol} = 0.01 s^{-1}. Hence, we could achieve our objectives for the steady state with assignment of k_{12} = 0.5 s^{-1} and D_G = 15.5 μm^2/s (**Fig. S5A**).

FRAP predictions were executed with the same equations as presented in the previous section; only r_{12} and values of common parameters are different as noted here. While one might think of conversion to the polymerizable state as a 'rate-limiting' step, the results show that FRAP is actually predicted to be comparable to that of the DODL scenario with one, lumped G-actin state (**Fig. S5B**). This is because diffusion and interconversion within the domain occur in parallel, in effect combining to speed up the approach to steady state.

6. Leading-eigenvalue analysis of DODL (constant- and variable-diffusivity) scenarios

The FRAP recovery results for DODL scenarios that might be counterintuitive are:

1) It is perhaps surprising that the recoveries are so fast. The $t_{0.5}$ value for the DODL (constant diffusivity) scenario presented in **Fig. 4** is roughly 1 order of magnitude lower than the characteristic timescale of diffusion, $t_D = L^2/D_{G,DODL(c)}$ = 9.5 s;

2) The variable-diffusivity cases of various forms and diffusivity gradients – subject to the same experimental constraints – yield very similar leading-edge FRAP kinetics.

A physical interpretation of observation 1 (duplicated from the main-text Discussion) considers that, at early times post-bleach, there is a steep, positive gradient of unbleached G-actin and an almost-as-steep, negative gradient of bleached G-actin in the *x*-direction. These sum to maintain the relatively modest, positive gradient of G-actin overall. Therefore, at early times post-bleach, the flux of unbleached G-actin is much greater than at steady state and dominated by diffusion. On a more quantitative level, we note that DODL, with constant G-actin diffusivity and no F-actin depolymerization, has a well-known analytical solution. For such a Dirichlet problem, the leading term of the infinite-series solution decays as $\exp(-t/\tau_1)$, where

$$\tau_1 = \frac{t_D}{\pi^2}$$

(with a time constant 10-fold lower than t_D). Incidentally, the $t_{0.5}$ value for the Dirichlet problem and our values of L = 10 μm and $D_{G,DODL(c)}$ = 10.5 μm^2/s is approximately 1.3 s and scales precisely with t_D. This value is only modestly lower (faster) than the $t_{0.5}$ values of our DODL predictions, which include the depolymerization reaction; in the scenarios considered, F-actin is fully bleached initially, and so this was expected.

To put this on a more formal basis, and to address observation 2 stated above, we cast the DODL problem (with possibly variable diffusivity) as follows.

$$\frac{\partial g_{un}}{\partial t} = \frac{\partial}{\partial x}\left[D_{G,DODL}(x)\frac{\partial g_{un}}{\partial x}\right] + k_{depol} f_{un};$$
$$g_{un}(x,0) = 0;$$
$$g_{un}(0,t) = 0;$$
$$g_{un}(L,t) = g(L).$$

Based on the reasoning above, we neglect the depolymerization term for early times; and, with a standard change of variables, we make the Dirichlet boundary conditions homogeneous:

$$g_{un}(x,t) = b(x) - y(x,t)$$
$$\frac{\partial y}{\partial t} = \frac{\partial}{\partial x}\left[D_{G,DODL}(x)\frac{\partial y}{\partial x}\right];$$
$$\frac{d}{dx}\left[D_{G,DODL}(x)\frac{db}{dx}\right] = 0;$$
$$y(x,0) = b(x);$$
$$y(0,t) = b(0) = 0;$$
$$y(L,t) = b(L) - g(L) = 0;$$

$$b(x) = g(L)\frac{\int_0^x \frac{dx'}{D_{G,DODL}(x')}}{\int_0^L \frac{dx'}{D_{G,DODL}(x')}}.$$

This now conforms to the general problem examined by Farkas and Deconinck (cited in the main text), who showed how to obtain estimates of the eigenvalues for the analogous problem in heat transfer, with variable thermal conductivity. Remarkably, analysis of their work reveals that the leading eigenvalue can be closely approximated by a simple function, such that the leading term of the solution decays with a characteristic diffusion timescale,

$$\tau_1 \approx \left(\frac{1}{\pi}\int_0^L \frac{dx'}{{D_{G,DODL}}^{\frac{1}{2}}(x')}\right)^2 = \left(\frac{L}{\pi}\langle {D_{G,DODL}}^{-\frac{1}{2}}(x)\rangle\right)^2.$$

For constant diffusivity, this matches the well-known result given above.

Given the same experimental inputs, both the constant- and variable-diffusivity DODL scenarios are subject to the same matching constraint, namely

$$V_F \int_0^{x_{match}} \frac{f(x')}{D_{G,DODL}(x')}\,dx' = g(x_{match}).$$

Because the steady-state F-actin profile, $f(x)$, is typically a weak function of x, all plausible $D_{G,DODL}(x)$ at least approximately obey

$$\int_0^L \frac{1}{D_{G,DODL}(x')}\,dx' \approx \frac{L}{D_{G,DODL(c)}}.$$

This explains why all DODL scenarios with sufficiently smooth functions $D_{G,DODL}(x)$ (including constant diffusivity) yield similar FRAP recovery kinetics; they have approximately the same value of

$$\langle {D_{G,DODL}}^{-1}(x)\rangle \approx \left(\langle {D_{G,DODL}}^{-\frac{1}{2}}(x)\rangle\right)^2.$$

SUPPLEMENTAL FIGURES

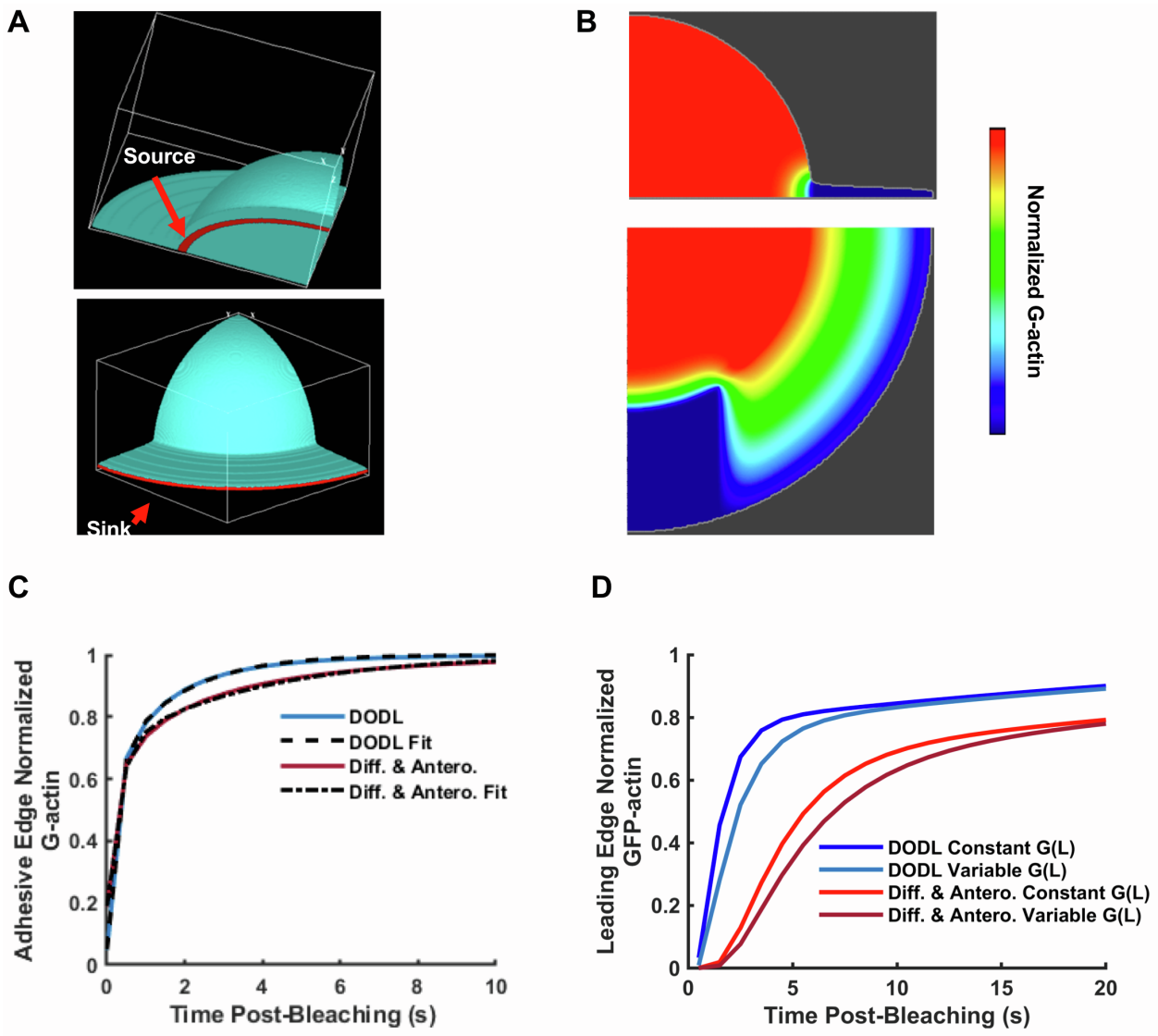

Figure S1. Additional analysis of FRAP model boundary conditions at $x = L$. (A) Reaction-diffusion equations were solved with a 3D geometry similar to those observed experimentally. A steady state G-actin concentration field was established by setting a constant-flux 'source,' localized in a ring pattern at the interface between adhesive and non-adhesive regions (top), and a first-order reaction 'sink' at the most-distal tip of the membrane (bottom). **(B)** G-actin concentration profiles in the YZ (x = 0) and XY (z close to the bottom) planes just after a simulated, 0.1 s bleach event. **(C)** FRAP time courses at the back and center of the bleached area were fit by a double-exponential function. **(D)** These functions were used in place of the constant-value boundary condition in 1D to generate new FRAP predictions.

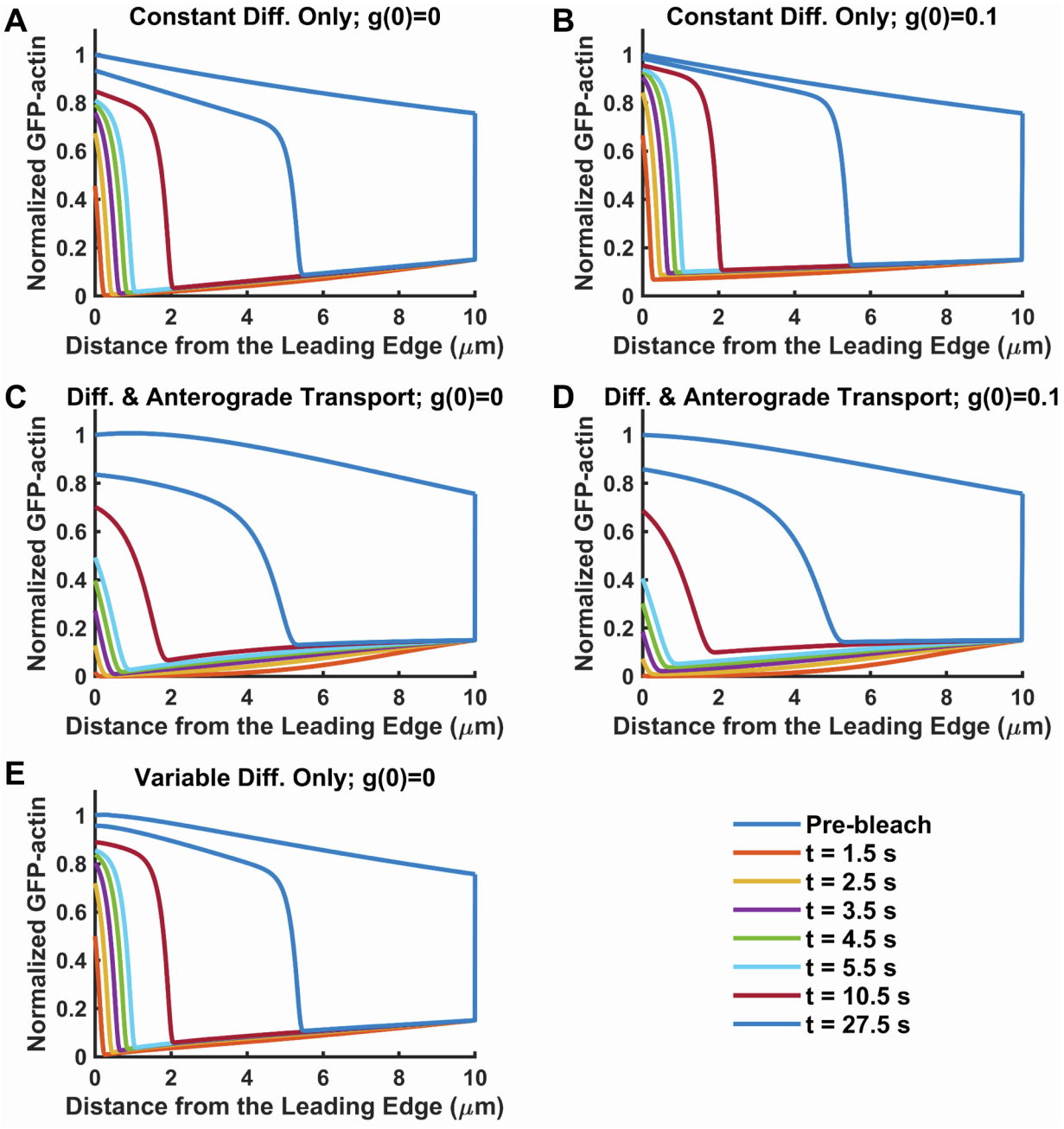

Figure S2. Pre- and post-bleaching line scans of total GFP-actin from 1D simulations. (A) Constant diffusion only (D_G = 10.5 μm^2/s) and $g(0)$ = 0.**(B)** Constant diffusion only (D_G = 29.7 μm^2/s) and $g(0)$ = 0.1. **(C)** Constant diffusion (D_G = 3 μm^2/s) aided by constant anterograde velocity and $g(0)$ = 0. **(D)** Constant diffusion (D_G = 3 μm^2/s) aided by constant anterograde velocity and $g(0)$ = 0.1. **(E)** Variable diffusion only ($D_G(0)$ = 3 μm^2/s).

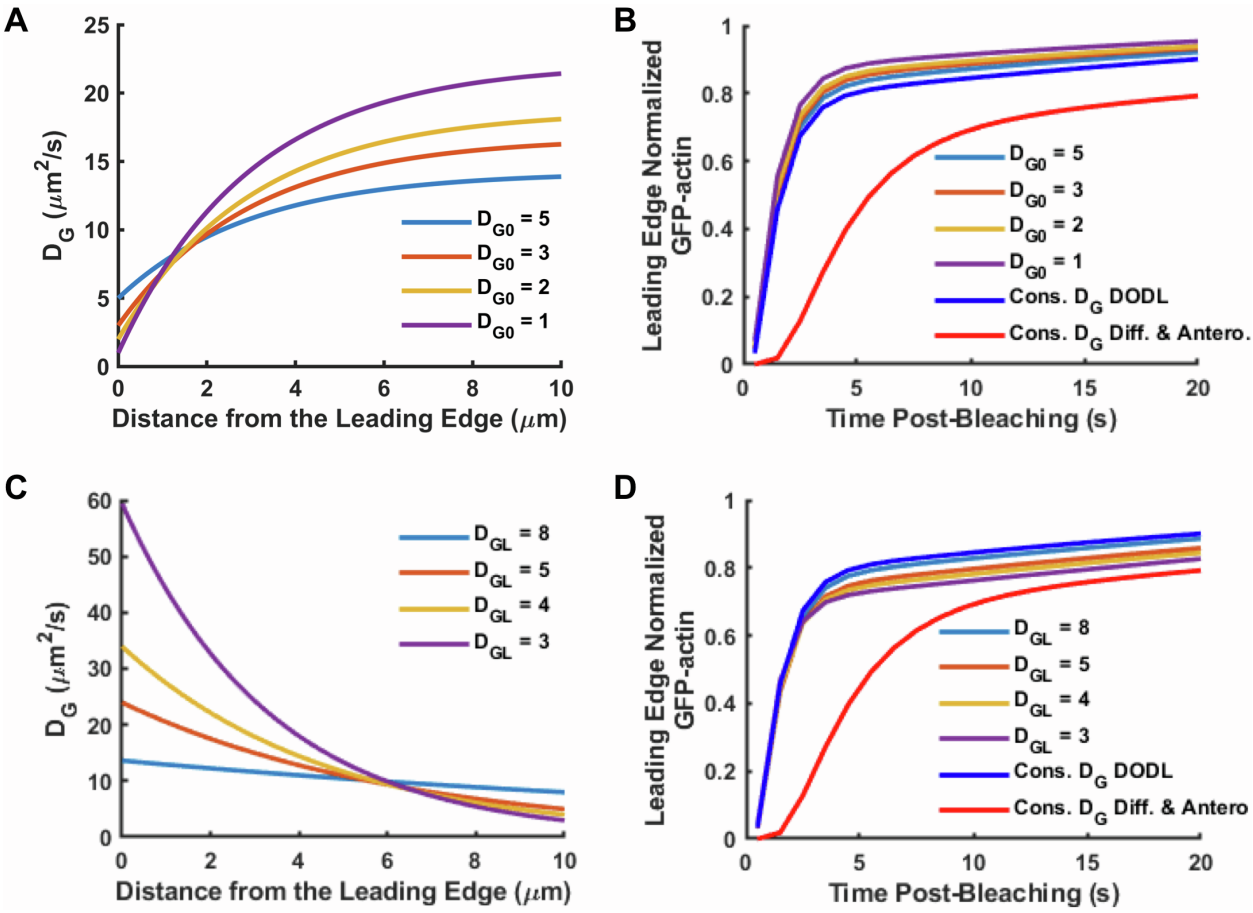

Figure S3. FRAP predictions for DODL scenarios with various $D_{G,DODL}(x)$. Under the same 1D simulation conditions described under **Fig. 4**, we simulated position-dependent G-actin diffusivity profiles that match the leading-edge flux and the G-actin concentrations at both boundaries. **(A)** Increasing diffusivity profiles, with the leading-edge value specified. **(B)** The variable-diffusivity DODL scenarios predict FRAP kinetics similar to the constant-diffusivity DODL scenario, unlike the scenario with $D_{G(c)}$ = 3 μm^2/s and V_G (Antero.) = 0.9 mm/s. **(C&D)** Same as **A**&**B**, respectively, except with decreasing diffusivity profiles and the values at $x = L$ specified.

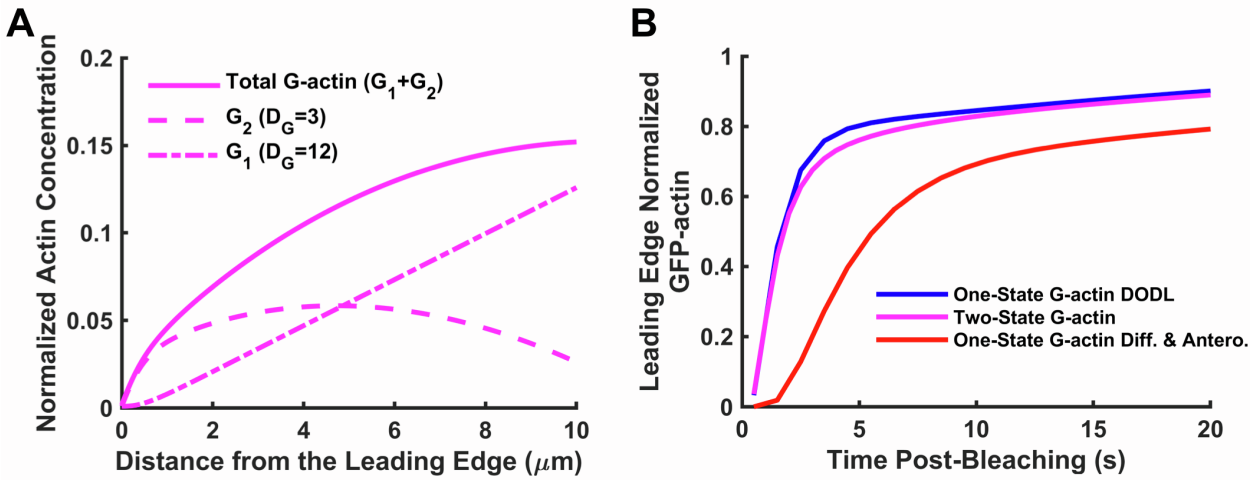

Figure S4. Modeling two states of G-actin with different diffusivities. (A) A slow diffusion of a polymerizable actin pool (G_2) can be offset by conversion from a fast-diffusing pool (G_1) to match steady-state observables. **(B)** The resulting FRAP prediction is nonetheless comparable to that of the 'one-state' DODL scenario, and thus much different from the scenario with constant, slow diffusivity plus anterograde, vectorial transport.

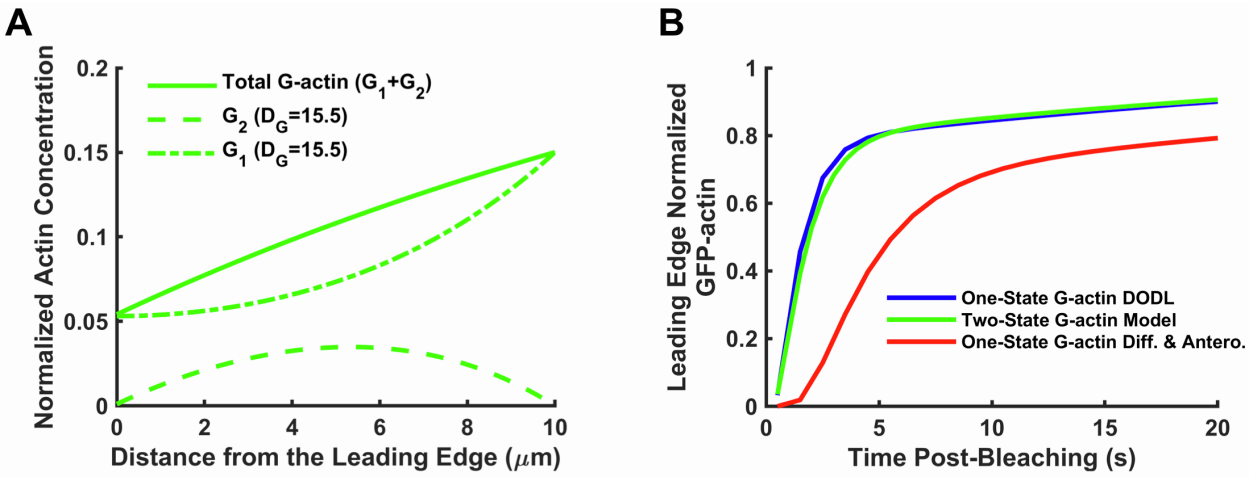

Figure S5. Modeling two states of G-actin with slow conversion to a polymerizable state. (A) With extreme values of parameters, a scenario with slow conversion to a polymerizable state (G_1 → G_2) can match steady-state observables. **(B)** The resulting FRAP prediction is nonetheless comparable to that of the 'one-state' DODL scenario, and thus much different from the scenario with constant, slow diffusivity plus anterograde, vectorial transport.

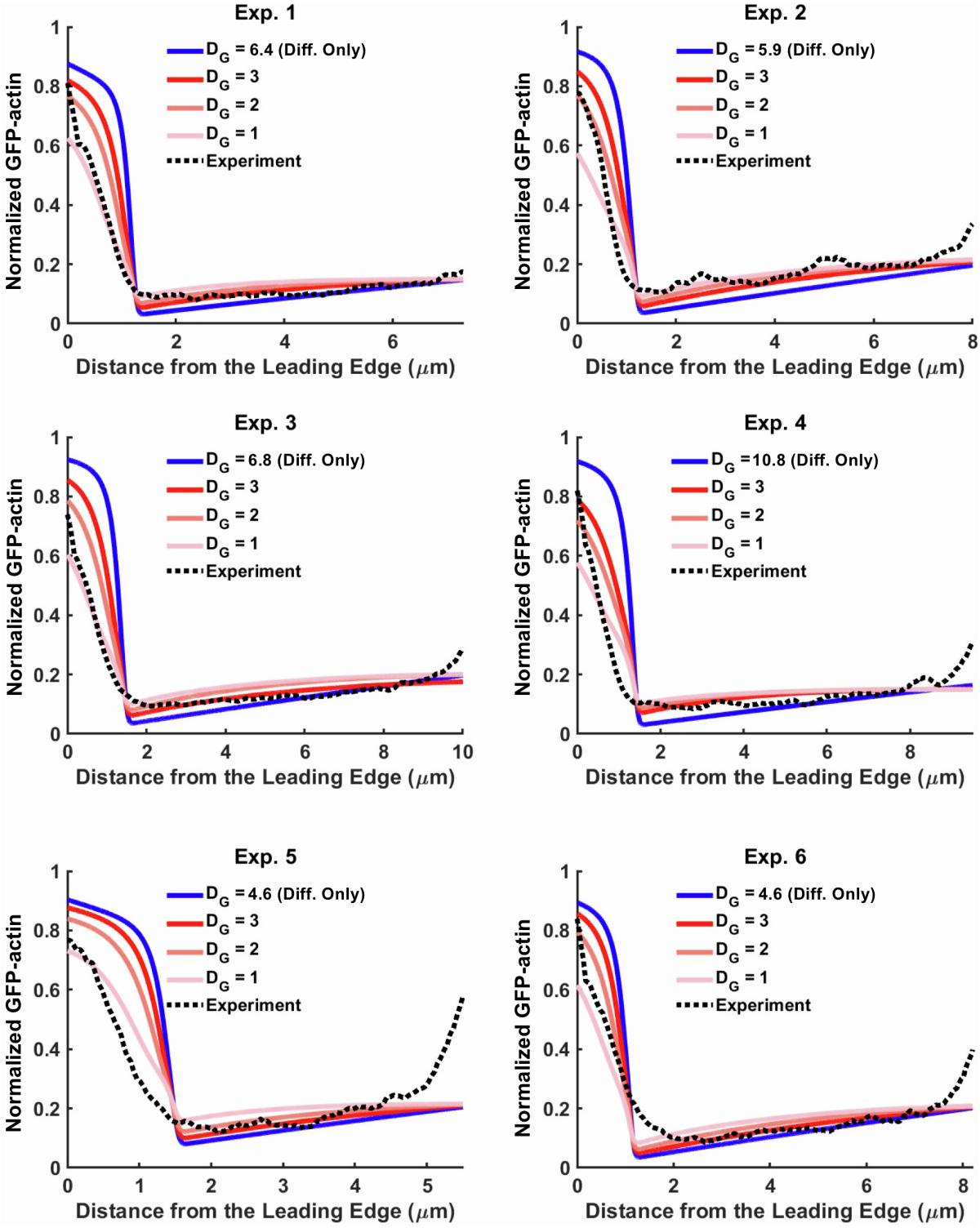

Figure S6. Spatial profiles measured at time = 2*$t_{0.5}$ do not align with the diffusion-only model predictions. Spatial profiles measured at 2*$t_{0.5}$ for six of the seven experiments (the seventh is shown in **Fig. 5C**) in the cohort and their corresponding simulation data for different values of D_G (μm^2/s).

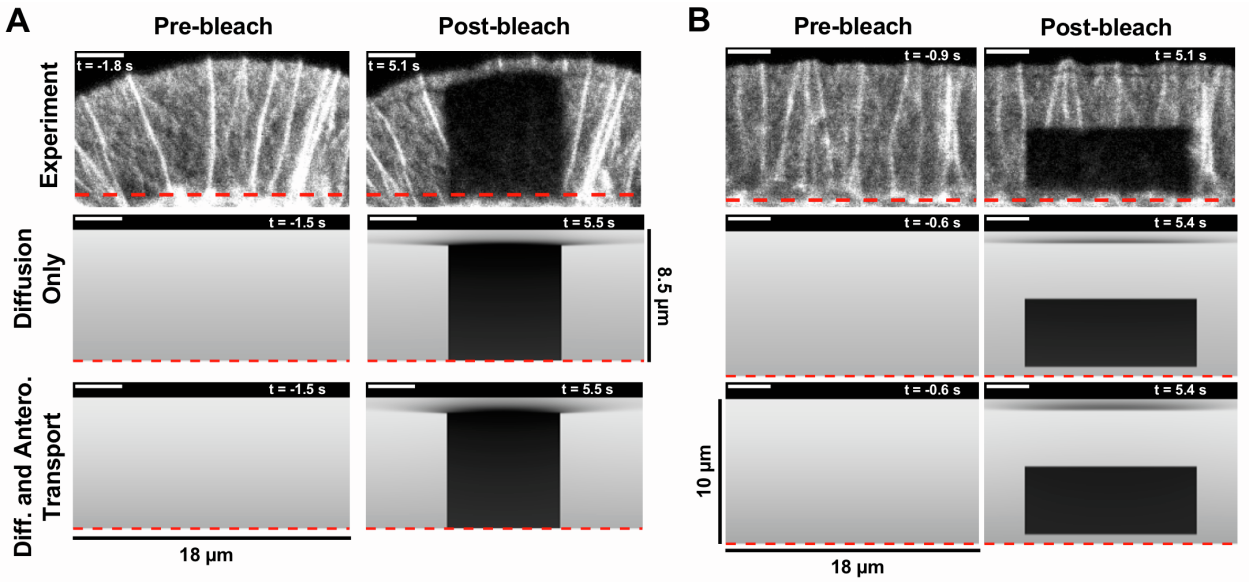

Figure S7. Simulated FRAP scenarios predict the rapid appearance of a thin, dark band, as observed in experiments. Following either full-span **(A)** or partial-span **(B)** bleaching, a thin dark band rapidly appears at the leading edge; because of isotropic G-actin diffusion, the band spreads laterally, outside the width of the bleached area. Model predictions for the key scenarios of DODL and diffusion plus advection (parameterized with $g(0) \approx 0$) are qualitatively consistent with experiments, but in this regard we were not able to discern the quantitative differences between the two scenarios from experiments.

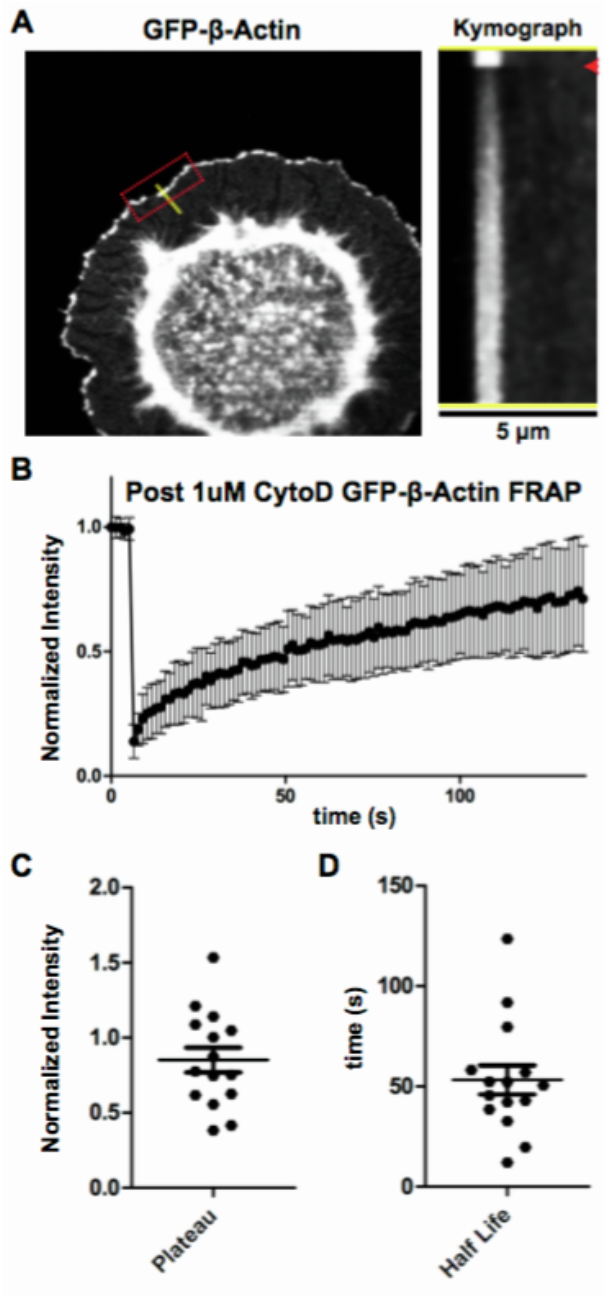

Figure S8. Dynamics of GFP-actin accumulating at spillover protrusion edges following CytoD treatment. (A) The same cell shown in **Fig. 6A**, with a dashed, red box indicating the photobleached region and a yellow line representative of the region from which the adjacent kymograph was generated (duration = 135 s). The red arrow in the kymograph marks when the bleach occurred. **(B)** FRAP recovery curves averaged across 15 cells bleached and monitored as depicted in **A**. Error bars represent the Standard Deviation of the Mean. **(C&D)** Plots of the plateau value (**C**) and half-life (**D**) of a one-phase exponential curve fitted to the FRAP curve of each cell included in the analysis shown in **B**.

CAPTIONS FOR SUPPLEMENTAL MOVIES

Movie S1. Supplemental movie for Figure 2A. Spillover protrusion labeled with GFP-actin bleached at a discrete region between the leading edge and the fibronectin attachment zone. Scale bar = 5 μm, and time stamp is in MM:SS format

Movie S2. Supplemental movie for Figure 2A. Spillover protrusion labeled with GFP-actin bleached in a wide stripe running all the way from the leading edge to the fibronectin attachment zone. Scale bar = 5 μm, and time stamp is in MM:SS format.

Movie S3. Supplemental movie for Figure 2C. JR20 Fibroblast expressing GFP-actin plated on a triangle micropatterned Fn island and bleached all throughout the spillover protrusion zone. Scale bar = 10 μm, and time stamp is in MM:SS format.

Movie S4. Supplemental movie for Figure 2C. JR20 Fibroblast expressing GFP-actin plated on a square micropatterned Fn island and bleached all throughout the cell body at and above the Fn attachment site. Scale bar = 10 μm, and time stamp is in MM:SS format.

Movie S5. Supplemental movie for Figure 6A. JR20 Fibroblast expressing GFP-actin plated on a circle micropatterned Fn island and treated with 1 μM between frames marked with 00:36 and 00:37. Scale = 10 μm and time stamp is in MM:SS format (there was a ~15-20s pause between 00:36 and 00:37 for drug wash in, which is not shown/accounted for in the time stamp).